Speed of traveling fronts in a sigmoidal reaction-diffusion system

E. P. Zemskov,[1,2,a)] K. Kassner,[3,b)] M. A. Tsyganov,[4,c)] and I. R. Epstein[1,d)]
[1]*Department of Chemistry, Brandeis University, MS 015, Waltham, Massachusetts 02454, USA*
[2]*Computing Centre, Russian Academy of Sciences, Vavilova 40, 119333 Moscow, Russia*
[3]*Institut für Theoretische Physik, Otto-von-Guericke-Universität, Universitätsplatz 2, 39106 Magdeburg, Germany*
[4]*Institute of Theoretical and Experimental Biophysics, Russian Academy of Sciences, Institutskaya 3, 142290 Pushchino, Moscow region, Russia*

(Received 28 June 2010; accepted 10 February 2011; published online 28 March 2011)

We study a sigmoidal version of the FitzHugh–Nagumo reaction-diffusion system based on an analytic description using piecewise linear approximations of the reaction kinetics. We completely describe the dynamics of wave fronts and discuss the properties of the speed equation. The speed diagrams show front bifurcations between branches with one, three, or five fronts that differ significantly from the classical FitzHugh–Nagumo model. We examine how the number of fronts and their speed vary with the model parameters. We also investigate numerically the stability of the front solutions in a case when five fronts exist. © *2011 American Institute of Physics*. [doi:10.1063/1.3562546]

The classic FitzHugh–Nagumo (FHN) equations have been widely studied as a model for wave propagation and pattern formation in excitable media such as neural and reaction-diffusion systems. In that model, the inhibitor or recovery variable, *v*, has linear kinetics. More sophisticated models employ a more realistic sigmoidal kinetics for *v*. Here, we study a sigmoidal FHN-type model modified by replacing the nonlinear terms in the kinetics of both variables by piecewise linear functions, which enables us to obtain analytic expressions for wavefronts and their speeds. We examine how the number of fronts and their dynamics vary with such model parameters as the excitation threshold of the activator variable and the ratios of kinetic time scales and diffusion coefficients between activator and inhibitor.

I. INTRODUCTION

The nonlinear dynamics of wave propagation and pattern formation in a wide variety of active media may be effectively described by reaction-diffusion equations.[1,2] The well-known FitzHugh–Nagumo (FHN) model[3,4] can be written in the form of two reaction-diffusion equations.

$$\frac{\partial u}{\partial t} = f(u,v) + D_u \frac{\partial^2 u}{\partial x^2} = u(1-u)(u-a) - v + D_u \frac{\partial^2 u}{\partial x^2}, \tag{1}$$

$$\frac{\partial v}{\partial t} = g(u,v) + D_v \frac{\partial^2 v}{\partial x^2} = \varepsilon(u-v) + D_v \frac{\partial^2 v}{\partial x^2}, \tag{2}$$

where u is usually referred to as the "activator" or the potential variable and v as the "inhibitor" or the recovery variable. The excitation threshold $0<a<1$, the ratio of the time scales $\varepsilon>0$, and the diffusion coefficients D_u and D_v are constants. This model is widely studied as a qualitative prototype for excitable systems in many biological[5] and chemical[6] contexts.

However, the FHN model provides a less than adequate description of some processes because of the linear response $g(u,v) \propto u - v$ in Eq. (2). More accurate models contain nonlinear reaction functions for both variables. A standard choice is the FHN model with a sigmoidal term.[7] This model is more complicated than the FHN system, but analytic treatment is possible when piecewise linear approximations[8,9] using the Heaviside step function $\theta(u-a)$ are substituted for both nonlinear terms. Such an approach was used by Tonnelier and Gerstner,[10] who investigated the system where the piecewise linear reaction function in the first equation approximates the cubic nonlinearity, whereas the terms in the second equation constitute a caricature of the sigmoidal function. The Tonnelier–Gerstner model does not contain any spatial degrees of freedom, i.e., there are no diffusive terms.

In this work, we consider a sigmoidal model with Tonnelier–Gerstner kinetics which allows pattern formation in the form of wave propagation; we include spatial coupling through diffusion. Our goal is to find traveling wave solutions and determine their speed in order to compare the dynamics with the well-known wave behavior in the classical FHN system. This research is an extension of our recent work[11] with piecewise linear models.

The reaction-diffusion system investigated here takes the form

$$\frac{\partial u}{\partial t} = f(u,v) + \frac{\partial^2 u}{\partial x^2} = -u - v + \theta(u-a) + \frac{\partial^2 u}{\partial x^2}, \tag{3}$$

[a)]Electronic mail: zemskov@brandeis.edu and zemskov@ccas.ru.
[b)]Electronic mail: klaus.kassner@ovgu.de.
[c)]Electronic mail: tsyganov@iteb.ru.
[d)]Electronic mail: epstein@brandeis.edu.

$$\frac{\partial v}{\partial t} = g(u,v) + D\frac{\partial^2 v}{\partial x^2} = -\varepsilon v + \alpha\theta(u-a) + D\frac{\partial^2 v}{\partial x^2}, \quad (4)$$

where ε, α, and D are positive constants. The null-clines for this model are shown in Fig. 1.

We see that Eq. (3) is identical to the first equation in the piecewise linear caricature[9] of the FHN system, whereas Eq. (4), the recovery equation, differs from the FHN case by the piecewise linear reaction function. Therefore, we focus our attention on changes in the model behavior resulting from variation of the parameters in the recovery equation, in order to compare our results with the FHN dynamics.

The paper is organized as follows. In Sec. II, we derive the front solutions of the model and discuss their bifurcation behavior and stability. In Sec. III, we give some conclusions, putting our model into the perspective of general models for neuron dynamics. While our results are clearly specific to the piecewise linear model considered, which is, we would point out, a nonlinear model—the sum of two solutions is not a solution—some features of what we derive here may retain their relevance in more general settings.

II. DYNAMICS OF TRAVELING FRONTS

Introducing the traveling-frame coordinate $\xi = x - ct$ in partial differential equations (PDEs) (3) and (4), where c is the wave speed, we obtain the ordinary differential equations (ODEs) for traveling waves

$$\frac{d^2u}{d\xi^2} + c\frac{du}{d\xi} - u - v + \theta(u-a) = 0, \quad (5)$$

$$D\frac{d^2v}{d\xi^2} + c\frac{dv}{d\xi} - \varepsilon v + \alpha\theta(u-a) = 0. \quad (6)$$

Inserting the standard ansatz $u(\xi) = A\ \exp(\lambda\xi)$, $v(\xi) = B\exp(\lambda\xi)$ in each of the domains $u < a$ and $u > a$ (whose extension in ξ is to be determined as part of the solution), we obtain an eigenvalue problem reducible to the following matrix equation:

$$\begin{pmatrix} \lambda^2 + c\lambda - 1 & -1 \\ 0 & D\lambda^2 + c\lambda - \varepsilon \end{pmatrix}\begin{pmatrix} A \\ B \end{pmatrix} = 0. \quad (7)$$

Nontrivial solutions exist only if λ is one of the four possible eigenvalues. Hence the general solution takes the form

$$v(\xi) = B_3 e^{\lambda_3\xi} + B_4 e^{\lambda_4\xi} + v^*, \quad (8)$$

$$u(\xi) = A_1 e^{\lambda_1\xi} + A_2 e^{\lambda_2\xi} + \frac{B_3}{\mu_3}e^{\lambda_3\xi} + \frac{B_4}{\mu_4}e^{\lambda_4\xi} + u^*, \quad (9)$$

where $\lambda_{1,2} = -c/2 \pm \sqrt{c^2/4+1}$ and $\lambda_{3,4} = (-c \pm \sqrt{c^2+4D\varepsilon})/(2D)$ are the eigenvalues of the characteristic equation, $\mu_{3,4} = c(1-1/D)\lambda_{3,4} + \varepsilon/D - 1$ and u^*, v^* are constants. There are two basic types of one-dimensional solitary excitations, fronts and pulses, in active media described by reaction-diffusion systems. Here we consider only front solutions. Hence, we restrict the values of α and ε so that they admit a situation where three fixed points—two of which are stable—exist in the phase plane (see Fig. 1), i.e., $1 - a > (\alpha/\varepsilon)$. The front in our piecewise linear model consists of two segments, one of which vanishes as $\xi \to -\infty$ and the other as $\xi \to \infty$. Because D and ε are positive, $\lambda_{1,3} > 0$ and $\lambda_{2,4} < 0$, and the solution has the form

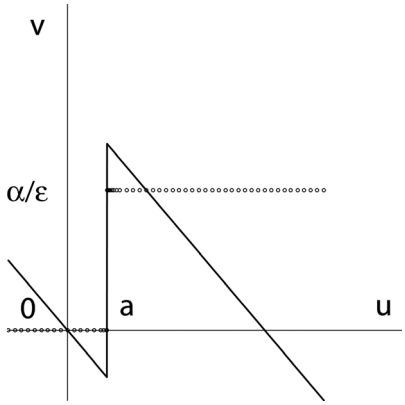

FIG. 1. Null-clines for the model (3) and (4), $f(u,v) = -u - v + \theta(u-a) = 0$ and $g(u,v) = -\varepsilon v + \alpha\theta(u-a) = 0$, are shown by solid lines and circles, respectively.

$$u(\xi) = \begin{cases} A_1 e^{\lambda_1\xi} + \dfrac{B_3}{\mu_3}e^{\lambda_3\xi}, & \xi \le \xi_a, \\ A_2 e^{\lambda_2\xi} + \dfrac{B_4}{\mu_4}e^{\lambda_4\xi} + 1 - \alpha/\varepsilon, & \xi \ge \xi_a, \end{cases} \quad (10)$$

$$v(\xi) = \begin{cases} B_3 e^{\lambda_3\xi}, & \xi \le \xi_a, \\ B_4 e^{\lambda_4\xi} + \alpha/\varepsilon, & \xi \ge \xi_a. \end{cases} \quad (11)$$

From the continuity of the $v(\xi)$ solution and its derivative at the matching point $\xi_a = 0$ (matching conditions) we find the two constants of integration for the recovery variable

$$B_3 = -\frac{\alpha}{\varepsilon}\frac{\lambda_4}{\lambda_3 - \lambda_4}, \quad B_4 = -\frac{\alpha}{\varepsilon}\frac{\lambda_3}{\lambda_3 - \lambda_4} \quad (12)$$

and from the continuity of the $u(\xi)$ solution and its derivative, and the equation fixing the matching point, $u(\xi_a) = a$, we obtain the other two integration constants

$$A_1 = a - \frac{B_3}{\mu_3}, \quad A_2 = a - \frac{B_4}{\mu_4} - 1 + \alpha/\varepsilon \quad (13)$$

and the speed equation

$$a = (\alpha/\varepsilon - 1)\frac{\lambda_2}{\lambda_1 - \lambda_2} - \frac{\alpha/\varepsilon}{(\lambda_1 - \lambda_2)(\lambda_3 - \lambda_4)}\left[\frac{\lambda_4}{\mu_3}(\lambda_1 - \lambda_3) - \frac{\lambda_3}{\mu_4}(\lambda_2 - \lambda_4)\right], \quad (14)$$

which gives the excitation threshold, a, as a function of the speed, which is contained in the λ and μ terms. When the Heavyside function, i.e., the term nonlinear in the variable u, is absent in the recovery equation, which corresponds to the case $\alpha = 0$, the v-front disappears, because $B_3 = B_4 = 0$ and the speed equation reduces to $a(\lambda_1 - \lambda_2) + \lambda_2 = 0$.

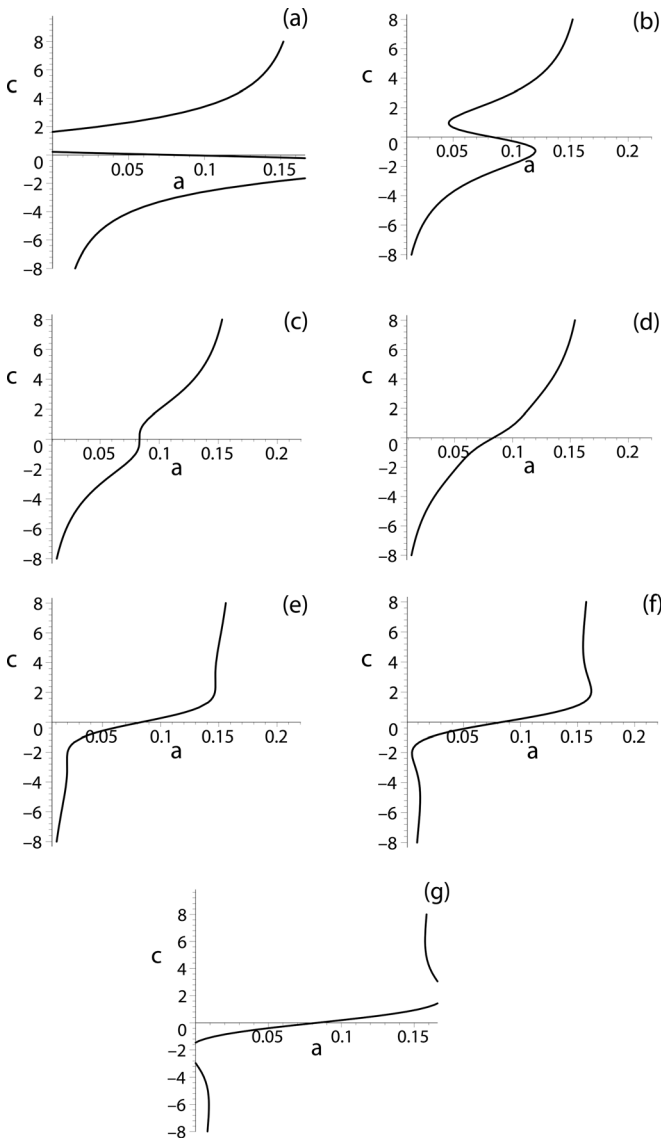

FIG. 2. Front speed c vs excitation threshold a relation described by Eq. (14) at (a) $D=1$, (b) $D=5$, (c) $D=8.2$, (d) $D=10$, (e) $D=15$, (f) $D=18$, and (g) $D=20$; $\varepsilon=0.12$; $\alpha=0.1$.

A. Speed diagrams

The behavior of the speed, c, as a function of the excitation threshold a is illustrated for several values of the diffusion constant ratio D in Fig. 2. When the diffusion constant of the recovery variable, v, is equal [Fig. 2(a)] or close to that of u, the speed curve consists of three disjoint segments, because the two turning points of the curve lie outside the interval $a \in (0, 1-\alpha/\varepsilon)$ in which two stable fixed points are present, i.e., the parameter region which can support the existence of a front. We note that all speed diagrams are symmetric about the midpoint of this a-interval, i.e., $c\left(\frac{1}{2}(1-\alpha/\varepsilon)-a\right) = -c\left(\frac{1}{2}(1-\alpha/\varepsilon)+a\right)$. This symmetry corresponds to the left–right symmetry of the model; at equal distances to the left and right of the midpoint $a^* = \frac{1}{2}(1-\alpha/\varepsilon)$, the model has wave solutions moving at the same speed in opposite directions. As the diffusion constant of the recovery variable grows, the speed curve moves inside the "front interval" [Fig. 2(b)], dividing the parameter space into two domains, one where the c–a relation has a single value and another where this relation is multivalued. When D is increased still further, the speed curve in the c–a plane unfolds [Figs. 2(c) and 2(d)]. This transition from multivalued behavior to a single value for the speed in the c–a plane reflects a pitchfork bifurcation in the c–D plane at a fixed value of a.

When the speed curve folds in the c–a plane, it forms three connected branches; the upper and lower branches correspond to the speeds of two counter propagating fronts and terminate at a critical value of a. A similar bifurcation scenario exists for the FHN system, where the bifurcation parameter is the ratio of the time scales, ε. This bifurcation has been referred to in the literature as a nonequilibrium Ising–Bloch bifurcation.[12–14] However, there exists a difference in our present bifurcation scenario: when D becomes large enough, the outer parts of speed curve fold [Figs. 2(e) and (2f)] in a manner similar to the folding of the inner part, so that finally their outer portions move outside of the front-supporting interval of a [Fig. 2(g)].

The scenario of bifurcations can be clearly seen when the extrema of the function $a=a(c)$, Eq. (14), described by the equation $da(c)/dc=0$, are plotted against the bifurcation parameter, the ratio D of the diffusion constants. The results are pictured in Fig. 3. The above-described scenario of front bifurcations related to the set of speed diagrams in Fig. 2 is depicted in Fig. 3(a), where the curve on the left side of the diagram corresponds to the inner folding, whereas the two curves on the right side reflect the folding of the two outer parts of the speed curve. The intermediate region without extrema is associated with the single valued portion of the speed curve. This scenario changes when the ratio, ε, of the time scales varies. For smaller values of ε, the separate curves on the left and right sides in Fig. 3(a) approach each other and connect [Fig. 3(b)]. At even lower ε, they separate to form three new curves [(Fig. 3(c)], so that there exists a multivalued speed curve in the *entire* region of D values.

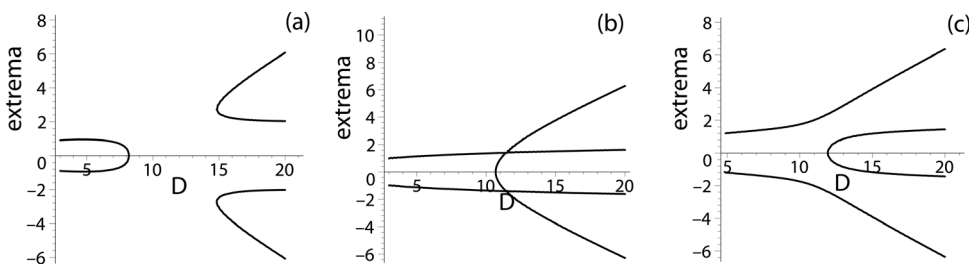

FIG. 3. Bifurcation scenarios. Extrema of the function $a=a\ (c)$ vs the ratio of diffusion constants, D, defined by the equation $da(c)/dc=0$ at (a) $\varepsilon=0.12$, (b) $\varepsilon=0.1093$, and (c) $\varepsilon=0.105$; $\alpha=0.1$. Panels (a), (b), and (c) show the behavior of extrema for parameter values related to Figs. 2, 4, and 5, respectively.

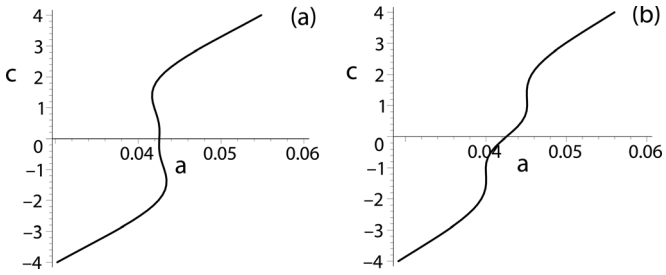

FIG. 4. Front speed, c, vs excitation threshold, a, according to Eq. (14) at (a) $D = 10.7$ and (b) $D = 11.1$. $\varepsilon = 0.1093$; $\alpha = 0.1$.

The speed curves at different values of ε and when $D \approx 10 - 13$ [Fig. 3(b)] are similar shape to the curves in Figs. 2(a) and 2(b) when $D \approx 1 - 5$ [Figs. 2(f) and 2(g)] and when $D \approx 18 - 20$.

Characteristic speed diagrams are presented in Figs. 4 and 5 for the scenarios in Figs. 3(b) and 3(c), respectively. Here, a new feature emerges: a second folding in the inner zone [Figs. 4(a) and 5(a)], so that *five* fronts are observed [Figs. 5(b) and 5(c)].

In Fig. 6, we give an example of front solution trajectories in the u–v plane. We show a case where five [see Fig. 5(c)] values of c exist. For the chosen parameter values ($a = 0.025, \varepsilon = 0.105, D = 12.7,$ and $\alpha = 0.1$), there are three fronts with positive and two with negative speed. Wave profiles $u = u(\xi)$ and $v = v(\xi)$ for one wave with a positive speed are presented in Fig. 7. They have a typical kink form for the activator–inhibitor pair.

B. Stability of waves. Numerical simulations

We present here a numerical investigation of the stability of the fronts with respect to the full PDEs (3) and (4). These results are obtained by straightforward numerical simulation of the system. The calculations are carried out for a

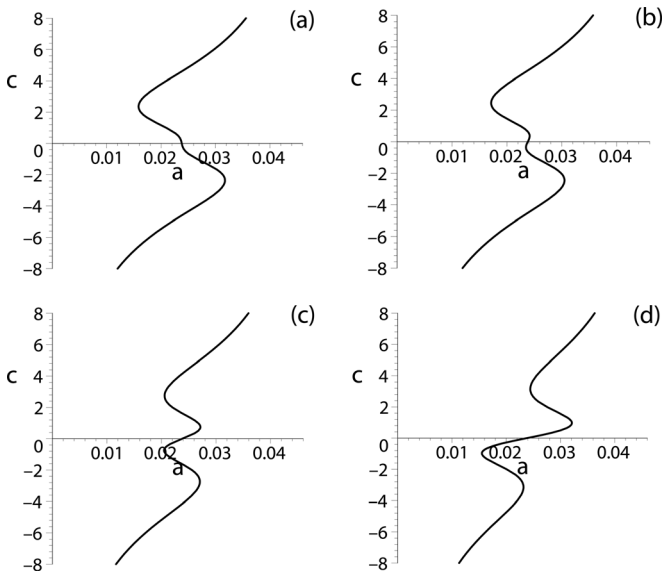

FIG. 5. Front speed, c, vs excitation threshold, a, Eq. (14), at (a) $D = 11.9$, (b) $D = 12.1$, (c) $D = 12.7$, and (d) $D = 13.5$. $\varepsilon = 0.105$; $\alpha = 0.1$.

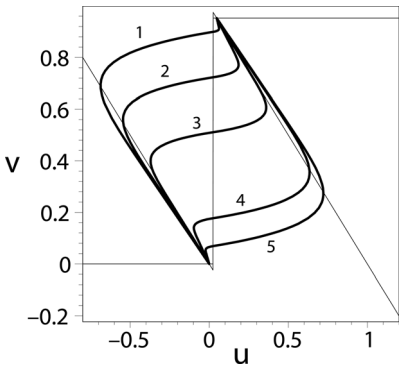

FIG. 6. Front waves (thick lines) in the u–v plane with speeds (1) $c \approx 4.474$, (2) $c \approx 1.399$, (3) $c \approx 0.169$, (4) $c \approx -1.861$, and (5) $c \approx -3.809$ for $a = 0.025$, $\varepsilon = 0.105$, $D = 12.7$, and $\alpha = 0.1$ [see Fig. 5(c)]. The null-clines, $f(u, v) = -u - v + \theta(u - a) = 0$ and $g(u, v) = -\varepsilon v + \alpha\theta(u - a) = 0$, are shown as thin lines.

one-dimensional medium of size $L = 160$ using the Euler method with no-flux boundary conditions

$$\left.\frac{\partial u}{\partial x}\right|_{x=0,L} = 0, \quad \left.\frac{\partial v}{\partial x}\right|_{x=0,L} = 0, \tag{15}$$

and with discretization steps $\delta x = 0.05$, $\delta t = 2 \cdot 10^{-5}$. The initial conditions are set as $u(x, 0) = u_0$ and $v(x, 0) = v_0$, where $x \in [0, L]$, by setting both variables to the resting state values. The wave was initiated at the left end of the interval with $u(x_{\text{init}}, 0) = u_{\text{init}}$ and $v(x_{\text{init}}, 0) = v_{\text{init}}$, where $x_{\text{init}} \in [0, x_0]$.

The results of these calculations are illustrated in Fig. 8, where we display the profiles of the u and v fronts. The numerical simulations performed for the case of motionless fronts [Fig. 8(a)] show good agreement with the theoretical results presented graphically in Fig. 7. The two moving fronts [Figs. 8(b) and 8(c)] have asymmetric profiles in accordance with our theoretical results obtained above. Thus, the numerical simulations show three distinct stable fronts at $a = 0.024$. The other two fronts are unstable, and cannot be obtained with any set of initial conditions. A complete linear stability analysis for the sigmoidal system can be extracted from the stability of the general system with a nonlinear inhibitor function.[11]

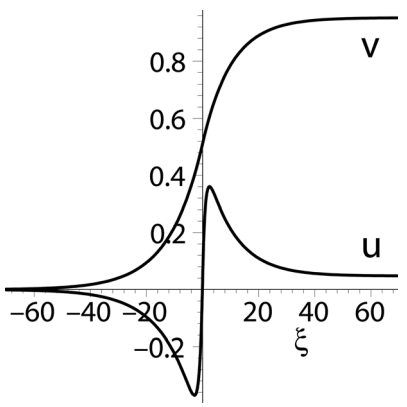

FIG. 7. Front profiles $u = u(\xi)$ and $v = v(\xi)$ with $c \approx 0.169$ for $a = 0.025$, $\varepsilon = 0.105$, $D = 12.7$, and $\alpha = 0.1$, corresponding to wave 3 in Fig. 6.

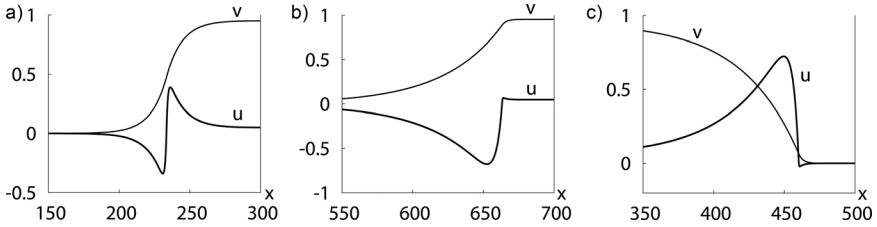

FIG. 8. Numerical simulations. Front profiles u and v for $\alpha = 0.1$, $\varepsilon = 0.105$, $D = 12.7$ and $a = 0.024$ at (a) $u_0 = 0.047$, $v_0 = 0.95$, $u_{\text{init}} = 0$, $v_{\text{init}} = 0$, $x_0 = 5$ with speed $c = 0$, (b) $u_0 = 0.047$, $v_0 = 0.95$, $u_{\text{init}} = 0$, $v_{\text{init}} = 0$, $x_0 = 2$ with speed $c \approx 4$, (c) $u_0 = 0$, $v_0 = 0$, $u_{\text{init}} = 1$, $v_{\text{init}} = 0$, $x_0 = 2$ with speed $c \approx 3.9$.

III. CONCLUSION

Originally, the FHN system was studied as a model for nerve conduction to understand the dynamics of the interaction between the membrane potential and the restoring force and to capture the basic properties of an excitable membrane. Most models of excitable membrane dynamics in computational neuroscience retain the general Hodgkin–Huxley format.[15] The FHN model is a two-component (u, v) simplification of the Hodgkin–Huxley system, where the membrane potential u and the recovery variable v mimic the dynamics of outward ionic transmembrane currents. The extension of the initial FHN model to more realistic systems where nonlinear inhibitor functions play a role is a topic that is receiving increasing attention in the last years.[7,16] One example is the Tonnelier–Gerstner[10] caricature of the the Morris–Lecar[17] model. The model developed by Morris and Lecar was used to describe oscillations in the giant muscle fiber of barnacles. Because it has biophysically meaningful and measurable parameters, the model has become quite popular in the computational neuroscience community. This model is more complicated than the FHN system, because all its equations are highly nonlinear. In order to make this system more tractable, Tonnelier and Gerstner[10] applied a piecewise linear approximation for the nonlinear terms.

The inclusion of diffusion effects into the Morris–Lecar model in the form of an infinite chain of diffusively coupled cells was made by Carpio.[18] In the context of neuronal activity, one of the important aspects of the synaptic organization of the cortex is the spatial location of a synapse on the dendritic tree of a neuron.[19] A single neuron produces a pulse that is transmitted to the others by synaptic coupling. The coupling is described by a linear resistance, so that the neuron assembly can be modeled by an array of nonlinear units with resistive (diffusive) connections.[20] Similarly, inclusion of the diffusive effects of a neuron's dendritic tree can also induce spatial pattern formation in a purely excitatory or inhibitory neural network.[21] Indeed, the cortex can be treated as a continuous 2D-sheet of neurons, which are labeled by continuous variables that give their spatial position on the sheet.[22] Introducing the average activity of neurons located at position x, one can describe the dynamics of the neuronal network in terms of the field equations for this spatial activity. These field equations have solutions in the form of complex stationary patterns, traveling waves, and rotating spirals–a phenomenology that is closely related to pattern formation in excitable media.[6,22]Caricatures of nonlinearities by steplike functions have much in their favor. The piecewise linear function used in this work provides insights into the most basic properties of propagating fronts and can, in many contexts, be considered as an adequate approximation for the more complicated nonlinear reaction functions in most real neuron models.[23,24] Alternatively, one may introduce a sigmoidal function of the tanh-type, which is sensitive to the current value of the activator variable. It can be used[25] as a smooth replacement for the Heaviside step function to distinguish between the excited and rest states of the neuron. Therefore, the reaction-diffusion model studied here may be considered as a starting point for more sophisticated investigations of the spatiotemporal dynamics in strongly nonlinear neuronal (excitable) media.

ACKNOWLEDGMENTS

The work of E.P.Z. was supported by the Russian Foundation for Basic Research (RFFI), project no. 07-01-00295. I.R.E. and E.P.Z. were supported by the U.S. National Science Foundation, Grant No. CHE-0526866.

[1]Y. Kuramoto, *Chemical Oscillations, Waves, and Turbulence* (Springer, Berlin, 1984).
[2]M. C. Cross and P. C. Hohenberg, Rev. Mod. Phys. **65**, 851 (1993).
[3]R. FitzHugh, Biophys. J. **1**, 445 (1961).
[4]J. Nagumo, S. Arimoto, and S. Yoshizawa, Proc. IRE **50**, 2061 (1962).
[5]J. D. Murray, *Mathematical Biology*, 3rd ed. (Springer, Berlin, 2003).
[6]A. S. Mikhailov and K. Showalter, Phys. Rep. **425**, 79 (2006).
[7]H. G. Rotstein, N. Kopell, A. M. Zhabotinsky, and I. R. Epstein, SIAM J. Appl. Math. **63**, 1998 (2003).
[8]H. P. McKean, Adv. Math. **4**, 209 (1970).
[9]J. Rinzel and J. B. Keller, Biophys. J. **13**, 1313 (1973).
[10]A. Tonnelier and W. Gerstner, Phys. Rev. E **67**, 021908 (2003).
[11]E. P. Zemskov and I. R. Epstein, Phys. Rev. E **82**, 026207 (2010).
[12]P. Coullet, J. Lega, B. Houchmanzadeh, and J. Lajzerowicz, Phys. Rev. Lett. **65**, 1352 (1990).
[13]A. Hagberg and E. Meron, Phys. Rev. E **48**, 705 (1993).
[14]A. Hagberg and E. Meron, Phys. Rev. Lett. **72**, 2494 (1994).
[15]A. L. Hodgkin and A. F. Huxley, J. Physiol. **117**, 500 (1952).
[16]H. Hardway and Y.-X. Li, Physica D **239**, 1650 (2010).
[17]C. Morris and H. Lecar, Biophys. J. **35**, 193 (1981).
[18]A. Carpio, Physica D **207**, 117 (2005).
[19]*The Synaptic Organization of the Brain*, edited by G. M. Shepherd (Oxford University Press, Oxford, 1990).
[20]V. B. Kazantsev, V. I. Nekorkin, S. Binczak, and J. M. Bilbault, Phys. Rev. E **68**, 017201 (2003).
[21]P. C. Bressloff, Phys. Rev. Lett. **76**, 4644 (1996).
[22]W. Gerstner and W. M. Kistler, *Spiking Neuron Models: Single Neurons, Populations, Plasticity* (Cambridge University Press, New York, 2002).
[23]V. B. Kazantsev, Phys. Rev. E **64**, 056210 (2001).
[24]S. Coombes, SIAM J. Appl. Dyn.. Syst. **7**, 1101 (2008).
[25]D. E. Postnov, F. Müller, R. B. Schuppner, and L. Schimansky-Geier, Phys. Rev. E **80**, 031921 (2009).